Journal of Materials Chemistry C

Accepted Manuscript

This article can be cited before page numbers have been issued, to do this please use: P. Singla, N. Van Steerteghem, N. Kaur, A. Z. Ashar, P. Kaur, K. Clays, K. S. Narayan and K. Singh, *J. Mater. Chem. C*, 2016, DOI: 10.1039/C6TC03876J.

View Article Online
DOI: 10.1039/C6TC03876J

Journal Name

ARTICLE

+Received 00th January 20xx,
Accepted 00th January 20xx

DOI: 10.1039/x0xx00000x

www.rsc.org/

Multifunctional geometrical isomers of ferrocene-benzo[1,2-b:4,5-b']difuran-2,6-(3*H*,7*H*)-dione adducts: Second-order nonlinear optical behaviour and charge transport in thin film OFET devices

Priya Singla,[a] Nick Van Steerteghem, [b] Navdeep Kaur,[a] A. Z. Ashar,[c] Paramjit Kaur,*[a] Koen Clays,[b] K. S. Narayan[c] and Kamaljit Singh*[a]

Geometrical isomers of a set of new ferrocene-benzo[1,2-b:4,5-b']difuran-2,6-(3*H,7H*)-dione dyads were synthesized and their optical, nonlinear optical (NLO) and electrochemical properties were investigated. The compounds were fully characterized with spectroscopic data and single crystal X-ray analysis in few cases. The second-order nonlinear polarizabilities were measured in chloroform using femtosecond hyper-Rayleigh scattering (HRS) method at 1300 nm. The dyads exhibit structure-dependent NLO properties, which could be rationalized by correlation with electrochemical and theoretical data. The (*Z*)-**6** chromophore recorded higher β_{HRS} than the corresponding (*E*)-**6** isomer, in the donor-acceptor (D-A) type dyads. Similarly, in D-A-D chromophore **7**, β_{HRS} values of isomers follow the order (*Z,Z*) > (*E,Z*) > (*E,E*), which matches with the trend of the wavelength of their maximum absorption as well as increasing band gap in that order. Owing to the inbuilt structural features, two of these D-A compounds were also explored as semiconducting materials in vacuum deposited top contact bottom gated thin film field-effect transistors (OFETs). Defying steric restrictions of ferrocene unit, the triad (*Z,Z*)-**7** depicted an unbalanced (μ_e: 3 x 10^{-3} $cm^{-2}V^{-1}s^{-1}$ and μ_h: 7 x 10^{-5} $cm^{-2}V^{-1}s^{-1}$) charge transport behaviour. Evaluation of the isomers of the type studied in this investigation constitute one of very few reports, in particular this study reveals for the first time semiconducting behaviour of thermally stable redox active Fc based semiconductors.

INTRODUCTION

Multifunctional organic materials[1] capable of performing different tailorable functions are in the forefront of future technologies. The donor-acceptor architects of π-conjugated compounds on one hand show optical nonlinearity, on the other hand these have been used in photovoltaics as well as thin film transistor devices etc.[2,3] Nonlinear optical (NLO)[4-7] materials have wide applications in the field of photonics,[8,9] nanophotonics[10] and optoelectronics,[11-14] such as optical signal processing, broad-band optical communications, integrated optics, optical sensing, optical poling, optical computing and optical limiting etc. and have received considerable recent interest. Out of a wide range of NLO active chromophores,[15-17] organometallic chromophores,[18-22] owing to their inbuilt structural features, redox behaviour, flexibility and ease of synthesis, thermal stability etc. constitute excellent candidates for potential applications in the field of electro-optical materials, photonics and semiconductors. This has additionally been attributed to their intense low energy electronic transitions originating from metal-to-ligand charge-transfer (MLCT) or ligand-to-metal charge-transfer (LMCT) transitions. Amongst the organometallics, ferrocene (Fc) owing to many attractive features such as electron donating strength and low oxidation potential facilitating the charge-transfer process, has presented itself as a good, tuneable electron donor alongside a variety of electron acceptors to probe NLO activity of the resulting various donor-acceptor (D-A) designs.[15-17] However, depending upon the oxidation state of the metal centre, the Fc unit can turn as a strong donor or acceptor, a feature that has been exploited for switching of the NLO activity, important in interfacing electronic data to wide band communication.[19,20,23-26] In our previous reports, we have deduced the structure-property relationships of NLO active chromophores by varying the conjugation path and/or acceptor strength.[25,27,28] Interestingly, in one of these reports, switching of the second-order NLO response of Fc push-pull chromophores was demonstrated.[25] Here in the present investigation, we report new class of dyads obtained by linking a donor Fc to benzo[1,2-b:4,5-b']difuran-2,6-(3*H*,7*H*)-dione acceptor to furnish D-A type

---

[a] *Department of Chemistry, UGC Centre of Advance Study-II, Guru Nanak Dev University, Amritsar – 143 005, India. E-mail: kamaljit.chem@gndu.ac.in (K. Singh), paramjit19in@yahoo.co.in (P. Kaur). Tel.: +91 183 2258853; fax: +91 183 2258819/20*

[b] *Department of Chemistry, University of Leuven, Celestijnenlaan 200D, B-3001 Leuven, Belgium. E-mail: Koen.Clays@fys.kuleuven.be (K. Clays).*

[c] *Chemistry and Physics of Materials Unit, Jawaharlal Nehru Centre for Advanced Scientific Research, Bangalore 560064, Karnataka, India.*

Electronic Supplementary Information (ESI) available: [X-ray crystallographic data, microanalytical data, cyclic voltammograms, cartesian coordinates of theoretically optimized geometries, contour diagrams and complete reference 44, CCDC 1499221 and 1499222]. For ESI and crystallographic data in CIF or other electronic format see DOI: 10.1039/x0xx00000x

View Article Online
DOI: 10.1039/C6TC03876J

dyad, or the D-A-D type chromophore, where the acceptor is flanked by two Fc units. Interestingly, we have isolated different geometrical isomers of the D-A constructs, which allowed us to deduce interesting comparisons on the NLO behaviour of these isomeric compounds. Despite of a significant number of studies reporting second order harmonic generation in Fc chromophores, only a few studies have been reported where such comparisons have been drawn.[29-34] Additionally, we explored charge transport behaviour of selected compounds in thin film organic field-effect transistor devices and found that these exhibit, both p-type as well as n-type charge transport behaviour.

EXPERIMENTAL SECTION

Materials and characterization

All liquid reagents were dried/purified by using the recommended drying agents and/or distilled over 4Å molecular sieves. Toluene was dried using sodium benzophenone ketyl. Ferrocene and benzoquinone were purchased from Spectrochem and used as such. IR spectrum was recorded on Perkin-Elmer FTIR-C92035 Fourier-transform spectrophotometer in range 400–4000 cm^{-1} as KBr pellets. ^{1}H NMR and ^{13}C NMR spectra were recorded on Bruker Biospin Avance III HD at 500 MHz, in $CDCl_3$ and/or DMSO-d_6 containing TMS as internal standard. Data are reported as follows: chemical shift in ppm (δ), integration, multiplicity (s = singlet, d = doublet, t = triplet, m = multiplet) and coupling constant J (Hz). Mass spectrum (HRMS) was recorded on Bruker HRMS MICROTOF II spectrometer. Melting points were recorded in open capillaries and are uncorrected. For column chromatography, silica gel (60–120 mesh) and (230-400 mesh) was employed and eluted with ethyl acetate/ hexane, chloroform/ hexane or dicloromethane/hexane mixtures. UV-visible studies were carried out using HITACHI U-2910 Spectrophotometer. The cell holder of the spectrophotometer was maintained at 25 °C for consistency in the recordings. The redox behaviour and the reversibility of the ferrocene/ferrocenium (Fc/Fc^+) redox couple were determined by cyclic voltammetry on a CHI 660D Electrochemical Workstation with a conventional three-electrode configuration consisting of glassy carbon electrode as working electrode, platinum wire as counter electrode and Ag/AgCl as the reference electrode. The experiments were carried out in a 1×10^{-4} M solution of sample in dichloromethane containing 0.025 M tetrabutylammoniumhexaflorophosphate, n-Bu_4NPF_6 as the supporting electrolyte at room temperature. Deoxygenation of the solutions was achieved by bubbling nitrogen for 10 min and the working electrode was cleaned after each run. The voltammograms were recorded with a scan rate of 100 mV s^{-1}. Thermogravimetric analyses (TGA) were performed (0–1000 °C) on an EXSTAR TG/DTA 6300 instrument under N_2 atmosphere, at a heating rate of 10 °C min^{-1}. Femtosecond HRS measurements[35-40] were performed at 1300 nm using a commercial Ti:sapphire laser at ambient temperature. Crystal violet (D_{3h}) in methanol was used as the reference, with a value of 434 x 10^{-30} esu at 1300 nm for the octopolar[41-43] β_{xxx} hyperpolarizability tensor component.

Computational methods

All theoretical calculations were carried out by using the Gaussian 09 suite of programs.[44] The molecular geometries of the chromophores and related calculations were performed by density functional theory (DFT) method using B3LYP functional group and 6-31G(d) as the basis set.[45,46] The first 15 excited states were calculated by using time-dependent density functional theory (TD-DFT calculations) in dichloromethane as the solvent medium (CPCM model). The molecular orbital contours were plotted using Gauss view 5.0.9. (For Cartesian co-ordinates see, Table S1-S5, see †ESI)

Fabrication and characterization of OFET devices

Top contact/ bottom gate geometry was adapted to fabricate FETs (with results represented from five devices of each of (*E*)-**6** and (*Z*,*Z*)-**7**). Glass substrates cut in definite sizes (1”×3/4”) were thoroughly cleaned by sonication in hot soapy water, deionized water, 1:1 mixture of isopropyl alcohol (IPA) and acetone. The substrates were then kept in a boiling mixture (100 °C) of ammonia, hydrogen peroxide and water (1:1:5) for 15 min. to get clean-hydrophilic substrates. The substrates were then cleaned in boiling IPA and made dry with N_2 gas flow. 40 nm thick aluminium gate electrodes were made on these substrates using thermal evaporation at 5×10^{-6} mbar. BCB dielectric in mesitylene was spin coated at 1000 rpm for 60 sec and is annealed at 290 °C for 2 h in N_2 filled glove box. Dielectric surface is then passivated with HMDS spin coated at 1000 rpm and annealed at 110 °C for 1 h. Molecules were slowly evaporated using programmed heater from a silica crucible at ~110 °C temperature and 3 x 10^{-5} mbar pressure, while keeping the substrate at room temperature. Thickness of the layer was monitored by quartz crystal monitor during the evaporation and was further verified by atomic force microscopy (AFM) studies. Source-drain Au contacts of thickness 40 nm and width ~2 mm were made using patterned mask and thermal evaporation at 5×10^{-6} mbar. Geometrical dimensions of OFET are in the range of channel length (L): 30-60 μm, channel width (W): 1-2 mm. OFET characterization were done in evacuated chamber connected with probes. OFET saturation mobility was calculated using the equation: $I_{ds} = [(\mu_{FET}^{sat} C_{ox}W)/2L](V_G-V_t)^2$, where I_{ds} is the saturation current, μ_{FET}^{sat} is the saturation mobility, C_{ox} is the capacitance per unit area of dielectric, W is the width of channel, V_G is the gate voltage, V_t is the threshold voltage and L is the length of the channel. Capacitance per unit area (C_{ox}) of a 400 nm thin film of divinyltetramethylsiloxane bisbenzocyclobutene (BCB) is measured as 2.1 nF/cm^2. Keithley 4200-SCS was used for electronic characterization of OFET. Atomic force microscopy (AFM) topographic images were taken using JPK Nanowizard 3 AFM in tapping mode (cantilever force constant: 40 N/m, resonant frequency: 310 kHz).

View Article Online
DOI: 10.1039/C6TC03826J

Synthesis

All compounds have been adequately characterized using spectroscopic as well as microanalytical data (Fig. S1-S27, see †ESI)

Synthesis of 2-2′-(2,5-dihydroxy-1,4-phenylene)diacetic acid 3

A three-necked round-bottomed flask equipped with two dropping funnels, was charged with ethyl cyanoacetate (8.50 g, 8 ml, 75 mmol) in ethanol (30 ml), to which concentrated ammonium hydroxide (6.37 g, 7 ml, 181.79 mmol) was added. Meanwhile, additional ethyl cyanoacetate (12.75 g, 12 ml, 112.76 mmol) and *p*-benzoquinone (10 g, 92.5 mmol) in ethanol (100 ml, 95%, *v*/*v*) was dissolved by stirring at 40 °C for 30 min. This solution was transferred to one of the dropping funnels while a dilute solution of ammonium hydroxide (22.75 g, 25 ml, 649.25 mmol) in water (40 ml) was added to the other dropping funnel. Stirring was started and the rates of addition of the dropping funnels was adjusted in such a way that the solutions were delivered into the flask at a uniform rate. After completion of the addition, the reaction mixture was stirred for additional 1 h. The precipitates formed were filtered under vacuum and washed with ethanol until the filtrate turned colourless. Compound **2** (7.5 g, 25%) was obtained as a dark purple solid.

For subsequent hydrolysis, a suspension of **2** (4 g, 12 mmol) in concentrated hydrochloric acid (0.037g, 25 ml, 1.02 mmol) and water (25 ml) was refluxed at 110 °C for about 20 h. To this hot reaction mixture, water (20 ml) and charcoal (2 g) were added and the reaction was stirred for additional 5 min, after which it was rapidly filtered under vacuum. The filtrate was cooled and **3** (2.8 g, 49%) was obtained as creamish white crystalline solid.

Synthesis of benzo[1,2-b-4,5-b′]difuran-2,6-(3*H,7H*)-dione 4

To a suspension of **3** (1.0 g, 4.10 mmol) in dry toluene (50 ml), acetic anhydride (10.82 g, 10 ml, 105.90 mmol) was added. The mixture was stirred at 100 °C for 5 h and the solvent was removed under reduced pressure. The residue was purified by column chromatography using chloroform as eluent and the product was recrystallized from toluene to obtain **4** (0.79 g, 64 %) as white crystalline solid. R_f: 0.20 (chloroform). m.p.: 260 °C. IR (KBr): υ_{max} 3096 (aromatic C-H str), 2925 (C-H str), 1787 (cyclic ester) cm^{-1}. ^1H NMR (500 MHz, DMSO, 25 °C): δ 3.96 (s, 4H, $-CH_2$), 7.24 (s, 2H, ArH). ^{13}C NMR (125 MHz, DMSO, 25 °C): δ 33.8, 107.8, 124.4, 150.6, 174.8. HRMS: m/z calculated for $C_{10}H_6O_4$: 190.0266. Found: 190.0000 (M^+).

Synthesis of ferrocene-1-carboxaldehyde 5

A mixture of N-methyl-formanilide (1.88 g, 1.90 ml, 14 mmol) and $POCl_3$ (1.35 g, 0.80 ml, 8 mmol), was stirred at 0 °C for 15 min. To the resultant suspension, finely powdered ferrocene (1.00 g, 0.005 mol) was added in small portions using a solid addition tube under the atmosphere of dry nitrogen gas. The resultant purple mixture was allowed to stir for additional 60 min. at room temperature until complete consumption of ferrocene was confirmed from the TLC. The reaction was quenched by the addition of cold aqueous sodium acetate (10% *w*/*v*) solution at 0 °C and allowed to stir overnight at room temperature and then extracted with diethyl ether (2 x 50 ml). The organic layer was treated, in sequence, with HCl (1N, 2 x 25 ml) solution, saturated aqueous sodium bicarbonate solution (2 x 25 ml) and water (3 x 25 ml), after which it was dried over anhydrous sodium sulphate. Finally the ether layer was evaporated under reduced pressure and the residue was purified by column chromatography using hexane:ethyl acetate (5:95, *v*/*v*) as eluents to afford ferrocene-1-carboxaldehyde **5** as a thick red oil. Upon recrystallization in hot hexane, **5** (1.10 g, 98%) was obtained as bright orange red crystalline solid. R_f: 0.15 (ethyl acetate:hexane/ 10:90). m.p.: 105 °C. IR (KBr): υ_{max} 3095 (aromatic C-H), 1660 (CHO), 1030 (Cp) cm^{-1}. ^1H NMR (500 MHz, $CDCl_3$, 25 °C): δ 4.19 (s, 5H, CpH), 4.38 (s, 2H, CpH), 4.47 (2H, CpH), 9.92 (s, 1H, CHO). ^{13}C NMR (125 MHz, $CDCl_3$, 25 °C): δ 66.4, 68.1, 68.9, 82.4, 192.5. HRMS: m/z calculated for $C_{11}H_{10}OFe$: 214.0081. Found: 213.8000 (M^+).

General procedure for synthesis of 3-(ferrocen-1-ylidene) benzo [1,2-b-4,5-b′]difuran-2,6-(3*H,7H*)-dione, 6 and 3,7-di-(ferrocen-1-ylidene)-benzo[1,2-b-4,5-b′]difuran-2,6-(3*H,7H*)-dione 7

A solution of benzo[1,2-b-4,5-b']difuran-2,6-(3*H*,7*H*)-dione **4** (0.50 g, 2.63 mmol), ferrocene-1-carboxaldehyde **5** (0.42 g, 1.90 mmol), and *p*-toluenesulfonic acid (*p*-TsOH) (0.08 g, 0.47 mmol) in acetic acid (25 ml) was refluxed at 115 °C in a two-neck round bottomed flask equipped with reflux condenser, under nitrogen atmosphere for 8 h. After completion (TLC), the reaction mixture was cooled to room temperature; water (30 ml) was added and was stirred for additional 15 min. This reaction mixture was then extracted with DCM (3 x 25 ml). The organic extract was washed with water (2 x 20 ml), dried over anhydrous sodium sulphate and evaporated under reduced pressure to obtain crude **6**, comprising of two isomers of the product in 33.68 and 66.31 % (^1H NMR, Fig. S28, see †ESI) ratio, respectively. The mixture was purified by column chromatography over 120-160 silica using chloroform:hexane (70:30 *v*/*v*) mixture as eluent and the isomeric product mixture was obtained in (0.25 g, 25%) yield. The isomers were resolved upon repeated (2-3 times) column chromatography over 230:400 silica using hexane:DCM (40:60, *v*/*v*) as eluent and the pure isomers (*Z*)-**6** and (*E*)-**6** were isolated as dark purple and dark red coloured solids, respectively.

Following a similar procedure, a refluxing (85 °C) solution of benzo[1,2-b-4,5-b']difuran-2,6-(3*H*,7*H*)-dione **4** (0.20 g, 1.05 mmol), ferrocene-1-carboxaldehyde **5** (0.49 g, 2.32 mmol), *p*-TsOH (0.051 g, 0.29 mmol) in acetic acid (15 ml) during 24 h, furnished crude **7**, which was purified over 120-160 mesh silica using chloroform:hexane (70:30 *v*/*v*) mixtures to isolate the isomeric products in (0.32 g, 52%) overall yield and 36.74%, 28.59% and 34.66% (^1H NMR, Fig. S29 and S30, see †ESI) ratio, respectively. The isomeric product mixture was resolved by repeated (2-3 times) column chromatography over 230:400 silica using hexane:DCM (50:50, *v*/*v*) as eluents to isolate pure isomers (*Z,Z*)-**7**, (*E,Z*)-**7** and (*E,E*)-**7** as dark green coloured solids. The characteristic data of the products is given below; however additional 2D NMR data is given in (Fig. S13-S17, see

View Article Online
DOI: 10.1039/C6TC03376J

†ESI). Further, to facilitate the ^{1}H NMR assignment, relevant protons are labelled (Fig. S1-S6, see †ESI).

3-(Ferrocen-1-ylidene)-benzo[1,2-b-4,5-b′]difuran-2,6-(3*H*,7*H*)-dione, (*Z*)-6

Purple solid. R_f: 0.38 (hexane:DCM/ 30:70). m.p. >280 ^{o}C. IR (KBr): υ_{max} 3084 (aromatic C-H), 3036 (=CH-), 2921 (-CH_2), 1763 (cyclic ester), 1039 (Cp) cm^{-1}. ^{1}H NMR (500 MHz, $CDCl_3$, 25 ^{o}C): δ 3.76 (s, $2H_g$, -CH_2), 4.24 (s, 5H, CpH 1), 4.74 (s, $2H_b$, CpH 2), 5.31 (s, $2H_c$, CpH 2), 7.02 (s, $1H_f$, ArH), 7.22 (s, $1H_d$, ArH), 7.51 (s, $1H_e$, =CH-). ^{13}C NMR (125 MHz, $CDCl_3$, 25 ^{o}C): δ 33.70, 70.25, 73.81, 73.85, 100.85, 107.51, 114.72, 122.15, 126.47, 143.84, 148.10, 150.96, 166.17, 173.62 HRMS: m/z calculated for $C_{21}H_{14}O_4Fe$: 386.0242 Found: 386.3416 (M^+).

3-(Ferrocen-1-ylidene)-benzo[1,2-b-4,5-b′]difuran-2,6-(3*H*,7*H*)-dione, (*E*)-6

Red solid. R_f: 0.33 (hexane:DCM/ 30:70). m.p. >280 ^{o}C. IR (KBr): υ_{max} 3079 (aromatic C-H), 3039 (=CH-), 2923 (-CH_2), 1770 (cyclic ester), 1035 (Cp) cm^{-1}. ^{1}H NMR (500 MHz, $CDCl_3$, 25 ^{o}C): δ 3.77 (s, $2H_g$, -CH_2), 4.27 (s, 5H, CpH 1), 4.73 (s, $2H_b$, CpH 2), 4.76 (s, $2H_c$, CpH 2), 7.08 (s, $1H_f$, ArH), 7.73 (s, $1H_d$, ArH), 7.78 (s, $1H_e$, =CH-). ^{13}C NMR (125 MHz, $CDCl_3$, 25 ^{o}C): δ 33.73, 70.33, 71.71, 72.96, 104.73, 107.70, 116.75, 123.15, 123.45, 143.98, 149.95, 150.58, 169.14, 173.28. HRMS: m/z calculated for $C_{21}H_{14}O_4Fe$: 386.0242 Found: 386.7609 (M^+).

3,7-Di-(ferrocen-1-ylidene)-benzo[1,2-b-4,5-b′]difuran-2,6-(3*H*,7*H*)-dione, (*Z*,*Z*)-7

Dark green solid. R_f: 0.67 (hexane:DCM/ 30:70). m.p. >280 ^{o}C. IR (KBr): υ_{max} 3098 (aromatic C-H), 3033 (=CH-), 1758 (cyclic ester), 1037 (Cp) cm^{-1}. ^{1}H NMR (500 MHz, $CDCl_3$, 25 ^{o}C): δ 4.24 (s, 10H, CpH 1), 4.73 (s, $4H_b$, CpH 2), 5.31 (s, $4H_c$, CpH 2), 7.16 (s, $2H_d$, ArH), 7.49 (s, $2H_e$, =CH-). ^{13}C NMR (125 MHz, $CDCl_3$, 25 ^{o}C): δ 70.25, 73.69, 73.76, 100.58, 115.56, 125.76, 142.60, 148.34, 166.34. HRMS: m/z calculated for $C_{32}H_{22}O_4Fe_2$: 582.0217 Found: 581.9723 (M^+).

3,7-Di-(ferrocen-1-ylidene)-benzo[1,2-b-4,5-b′]difuran-2,6-(3*H*,7*H*)-dione, (*E*,*Z*)-7

Dark green solid. R_f: 0.62 (hexane:DCM/ 30:70). m.p. >280 ^{o}C IR (KBr): υ_{max} 3083 (aromatic C-H), 3039 (=CH-), 1764 (cyclic ester), 1030 (Cp) cm^{-1}. ^{1}H NMR (500 MHz, $CDCl_3$, 25 ^{o}C): δ 4.25 (s, 5H, CpH 1), 4.27 (s, 5H, CpH 1′), 4.73 (s, $2H_b$, CpH 2), 4.75 (s, $2H_b$′, CpH 2′), 4.78 (s, $2H_c$′, CpH 2′), 5.32 (s, $2H_c$, CpH 2), 7.22 (s, $1H_d$, ArH), 7.52 (s, $1H_e$, =CH-), 7.71 (s, $1H_d$′, ArH′), 7.75 (s, $1H_e$′, =CH′-). ^{13}C NMR (125 MHz, $CDCl_3$, 25 ^{o}C): δ 70.26, 70.33, 71.70, 72.87, 73.89, 73.95, 100.71, 104.55, 115.22, 117.42, 122.19, 126.80, 142.60, 143.54, 147.80, 150.15, 166.35, 169.61. HRMS: m/z calculated for $C_{32}H_{22}O_4Fe_2$: 582.0217 Found: 581.9733 (M^+).

3,7-Di-(ferrocen-1-ylidene)-benzo[1,2-b-4,5-b′]difuran-2,6-(3*H*,7*H*)-dione, (*E*,*E*)-7

Dark green solid. R_f: 0.59 (hexane:DCM/ 30:70). m.p. >280 ^{o}C. IR (KBr): υ_{max} 3093 (aromatic C-H), 3039 (=CH-), 1767 (cyclic ester), 1045 (Cp) cm^{-1}. ^{1}H NMR (500 MHz, $CDCl_3$, 25 ^{o}C): δ 4.28 (s, 10H, CpH 1), 4.76 (s, $4H_b$, CpH 2), 4.80 (s, $4H_c$, CpH 2), 7.74 (s, $2H_d$, ArH), 7.77 (s, $2H_e$, =CH-). ^{13}C NMR (125 MHz, $CDCl_3$, 25 ^{o}C): δ 70.39, 71.80, 73.10, 104.61, 117.08, 123.25, 143.50, 149.65, 169.34. HRMS: m/z calculated for $C_{32}H_{22}O_4Fe_2$: 582.0217 Found: 581.9727 (M^+).

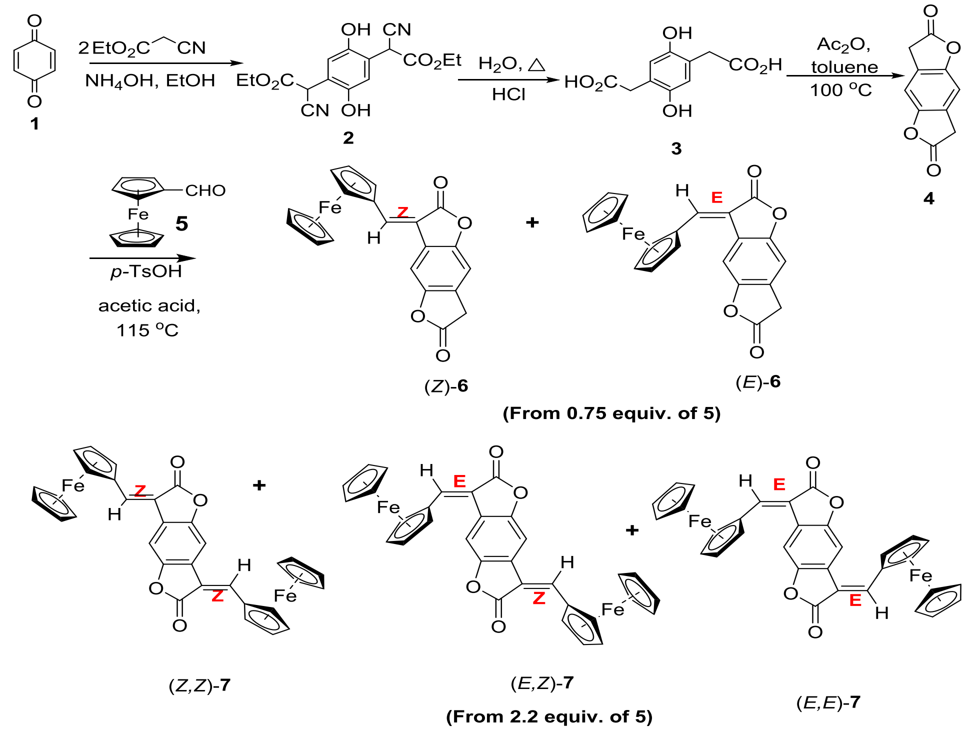

Scheme1: Synthesis of isomers of **6** and **7**.

View Article Online
DOI: 10.1039/C6TC03876J

RESULTS AND DISCUSSION

Synthesis

Condensation of ferrocene 1-carboxaldehyde **5** (2.2 equiv.) with benzo[1,2-b:4,5-b′]difuran-2,6-(3*H*,7*H*)-dione **4** using *p*-toluenesulphonic acid in acetic acid furnished isomeric mixture of 3,7-di-(ferrocen-1-ylidene)-benzo[1,2-b-4,5-b′]difuran-2,6-(3*H*,7*H*)-dione **7**, which were isolated after rigorous flash chromatography and identified as (*Z,Z*), (*E,Z*) and (*E,E*) isomers (Scheme 1) corresponding to D-A-D architect. However, when 0.75 equiv. of **5** were employed, *Z* and *E* isomers of the D-A type 3-(ferrocen-1-ylidene)-benzo[1,2-b-4,5-b′]difuran-2,6-(3H,7H)-dione **6** were isolated (Scheme 1). Compound **4** was prepared by subjecting 2,2′-(2,5-dihydroxy-1,4-phenylene) diacetic acid **3** to a dehydration reaction using acetic anhydride following a reported procedure.[47-49] Compound **3** in turn was obtained through condensation of 1,4-benzoquinone and ethyl cyanoacetate using ammonium hydroxide as base.[50] Selected compounds (*E*)-**6** and (*Z,Z*)-**7** showed good thermal stability with a decomposition temperature of 251 °C and 254 °C respectively (Fig. S31 and S32, see †ESI). The structures and geometry of (*Z*)-**6** and (*E,E*)-**7** isomers have additionally been confirmed by single crystal X-ray crystallography, while the geometries of the remaining isomers were assigned in analogy with the single crystal X-ray structures.

Theoretical study

We initiated our study on **6** (D-A) and **7** (D-A-D) compounds by first conducting a theoretical calculations (Gaussian09, B3LYP/6-31G(d))[44-46] for both, on the individual donor and acceptor molecules as well as their isomers, to visualize the density functional theory (DFT) optimized molecular geometries (Fig. S33, see †ESI) and charge density isosurfaces for the highest occupied molecular orbitals (HOMOs) and lowest unoccupied molecular orbitals (LUMOs) (Fig. 1) as well as their associated energies (Fig. S34 and S35, Table S6 and S7, see †ESI). Both **6** as well as **7** maintain the coplanarity of the benzodifuranone unit due to rigid C=C bonds of the molecular core flanked by one and two Fc units, respectively. The electron density in the HOMO-1 is exclusively localized on the donor Fc unit(s), while it is additionally distributed over the π-conjugated framework in the HOMO (Fig. 1) orbitals, both in **6** as well as **7**. It is localized on the acceptor benzodifuranone part in the LUMO and LUMO+1 orbitals indicating greater electron affinity. This unequivocally supports existence of charge transfer considering appropriate HOMO and LUMO.

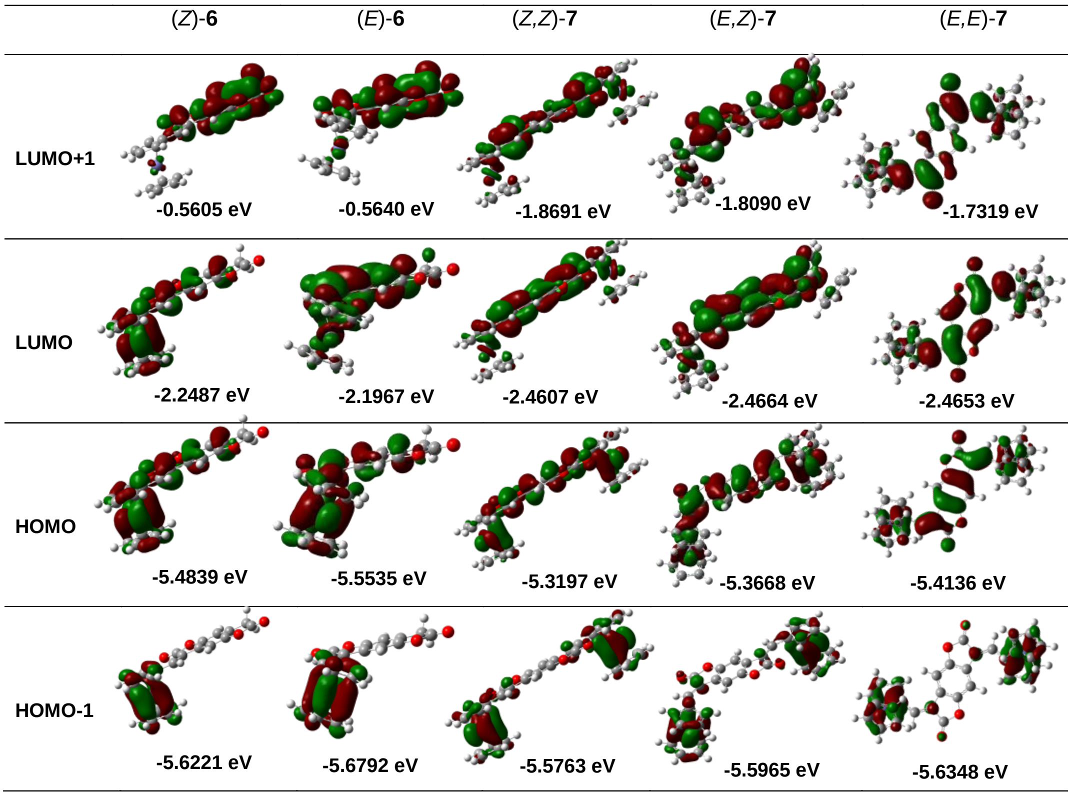

Fig. 1 Contour surfaces of frontier molecular orbitals involved in electronic transitions of HE bands of the isomers of **6** and **7**, obtained from TD-DFT calculations using B3LYP/6-31G(d) in DCM as solvent at an isosurface value of 0.02 au.

View Article Online
DOI: 10.1039/C6TC03876J

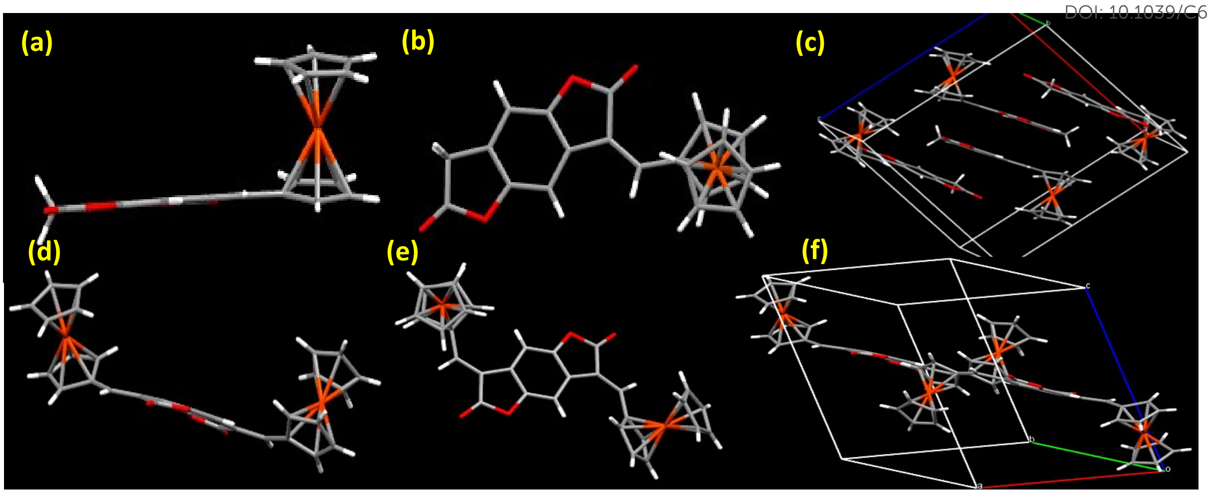

Fig. 2 ORTEP diagrams of (*Z*)-**6** and (*E,E*)-**7**: (a-c) side view, front view and crystal packing diagram of (*Z*)-**6**; (d-f) side view, front view and crystal packing diagram of (*E,E*)-**7.**

Single crystal X-ray structures of (*Z*)-6 and (*E,E*)-7

Crystals of both (*Z*)-**6** and (*E,E*)-**7** suitable for single crystal structural analysis could conveniently be grown by slow evaporation of their respective solutions (hexane:DCM/4:6 v/v) at room temperature. ORTEP diagrams of the side and front views and crystal packing structures are shown in fig. 2. The refinement details, bond lengths, bond angles and other crystallographic data are tabulated (Tables S8-S19, see †ESI). The chromophore (*Z*)-**6** crystallised in centrosymmetric monoclinic P lattice with P21/c space group and has an almost perfect coplanar arrangement between the Fc donor and the acceptor. The two Cp rings are slightly tilted (0.47°) w.r.t each other. The crystal packing structure (Fig. 2c) indicates that the dimer pairs adopt a head to tail (D-A…A-D) alignment in which the molecular dipoles are aligned antiparallel w.r.t each other.[30]

The chromophore (*E,E*)-**7** crystallised in centrosymmetric triclinic P lattice with P-1 space group with the two Cp rings of each Fc group tilted (1.14°) w.r.t each other. While the acceptor unit in both the cases maintain planarity, the two Fc units in the latter case point to the same side w.r.t the molecular plane of the central acceptor but are slightly tilted w.r.t each other (Fig. 2d). In the packing diagram, contrary to (*Z*)-**6**, one Fc group out of the two of one D-A-D **7**, slightly overlaps with a Fc group of the second molecule of the **7**, thus leading to a shifted stacking pattern.

Linear optical data

The UV-visible absorption spectra of both (*Z*)- and (*E*)-**6** (Fig. 3) are characterised by broad low energy (LE) bands in the range of 458-624 nm and relatively intense high energy (HE) bands in the range of 278-458 nm. In order to get a deeper insight into the contributing transitions to these absorption bands, time dependent density functional theory (TD-DFT) calculations were performed using B3LYP/6-31G(d) basis set using CPCM model in dichloromethane (DCM) phase. The TD-DFT deduced frontier molecular orbitals (FMOs) of the isomers (*Z*)- and (*E*)-**6** and their associated energies are depicted in fig. 4. The LE band at 542 nm in (*Z*)-**6** is essentially a MLCT band comprising of mainly: H→L (CI = 0.5156), H-3→L (CI = 0.4285) and H-1→L+3 (0.3687), while the HE bands at 386 and 328 nm are assigned as π→π* transitions with some contribution from MLCT also. The positions of these bands get blue shifted in (*E*)-**6** with LE band (H→L, CI = 0.4731) appearing at 528 nm and the HE bands at 380 and 320 nm, which may be due to the influence of the *trans*- geometry weakening the charge-transfer in (*E*)-**6** as compared to its *cis*- counterpart. Further, the LE bands depicted a large hypsochromic shift (Δλ=14 nm) in comparison to HE bands (Δλ= 6-8 nm) while moving from (*Z*)-**6** to (*E*)-**6**.

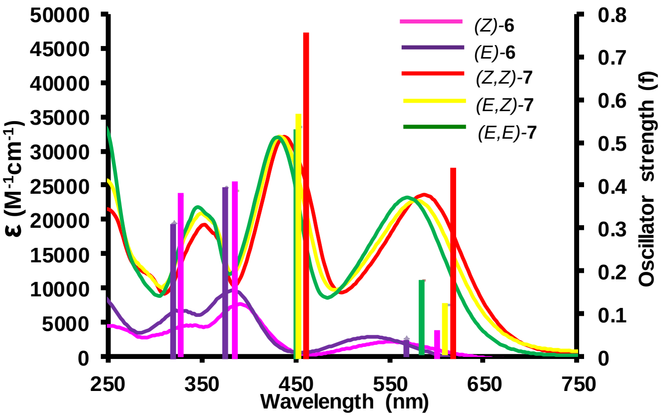

Fig. 3 Overlay of UV-visible absorption spectra in DCM (1 x 10^{-5} M) at 293 K, and oscillator strength calculated from DFT calculations using B3LYP/6-31G(d) in DCM phase, of isomers of **6** and **7**.

View Article Online
DOI: 10.1039/C6TC03876J

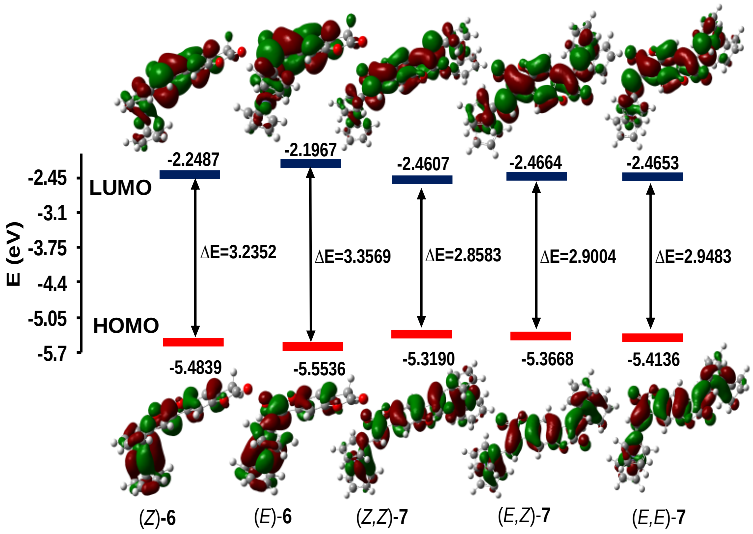

Fig. 4 Comparison of the TD-DFT (B3LYP/6-31G(d)/DCM phase) calculated energies of the FMOs and HOMO-LUMO band gaps (ΔE) of isomers of **6** and **7**.

The theoretical data furnished supporting evidence to the observed blue shift, as the calculated energy of the HOMO of (*E*)-**6** is less than that of (*Z*)-**6**, whereas the energies of the LUMO of (*E*)-**6** is raised in comparison to (*Z*)-**6** leading to increased band gap in (*E*)-**6** and consequent blue shift in the absorption band (Tables S20 and S21, see †ESI).

Similar spectral behaviour is observed in the isomers of **7**. The LE and HE bands of the three isolated isomers of **7** were in the range 494-734 nm and 302-494 nm, respectively (Fig. 3) and the energies of their FMO are plotted in fig. 4. It can be seen that the isomers with preponderance of (*Z*)- stereochemistry exhibit MLCT (LE) bands in the order: (*Z,Z*) > (*E,Z*) > (*E,E*) (λ_{abs}= 582, 570 and 568 nm, respectively). This is in good agreement with the predicted band gap (Fig.4) which follows the reverse order of λ_{abs} (Fig. 3 and Table S20, see †ESI). Similarly trends could be traced for the HE bands (π→π* transition) also (Table S20, see †ESI).

Electrochemistry

All isomers of chromophores **6** and **7** show electrochemically reversible oxidation peaks (Table 1 and Fig. S36, see †ESI) in analogy with the redox behaviour of Fc. Chromophore (*Z*)-**6** shows an anodic shift in the $E_{1/2}$ in comparison to Fc ($\Delta E_{1/2}$ = 0.100 V) reflecting the effect of electron withdrawal by benzo[1,2-b:4,5-b']difuran-2,6-(3*H*,7*H*)-dione acceptor rendering Fc more difficult to oxidize. The (*E*)-**6** isomer however saw a greater anodic shift ((*Z*)-**6**→(*E*)-**6**, $\Delta E_{1/2}$ = 0.059 V) (Table 1). This anodic shift is attributed to stabilization of the HOMOs of (*E*)-**6** (Table 1) compared to (*Z*)-**6**. Similar trend is observed upon comparing isomers of chromophore **7**, where the order of oxidation potential as well as half wave potential of the three isomers follow the order: (*Z,Z*) < (*E,Z*) < (*E,E*) [($\Delta E_{1/2}$ = 0.046V, Fc→(*Z,Z*)-**7**; 0.078V, (*Z,Z*)-**7**→(*E,Z*)-**7**; 0.113V, (*Z,Z*)-**7**→(*E,E*)-**7**) (Table 1)]. These observations are also in good agreement with the calculated energies of the corresponding HOMO's (Table 1).

Quadratic hyperpolarizability

The first hyperpolarisability β, of the isomers of chromophores **6** and **7** was measured in chloroform using the femtosecond hyper-Rayleigh scattering (HRS) method[35-40] at 1300 nm. Chromophore (*Z*)-**6** recorded higher β_{HRS} (52 x 10^{-30} esu) than

Table 1. HOMO-LUMO energies, band gaps and electrochemical data of isomers of **6** and **7**.

	E_{HOMO} (eV)[a]	E_{LUMO} (eV)[a]	E_g (eV)[a]	μ(D)[a]	E_{HOMO} (eV)[b]	E_{LUMO} (eV)[b]	E_g^{opt} (eV)[c]	λ_{edge} (nm)[d]	E_{pa} (V)[e]	$E_{1/2}$ (V)[f]	i_{pa} x 10^{-6} (A)[g]
(*Z*)-**6**	-5.580 (-5.484)	-2.303 (-2.249)	3.277 (3.235)	3.1308 (3.6327)	-4.950	-3.005	1.945	637.5	0.667 (0.577)	0.622	-1.793 (3.066)
(*E*)-**6**	-5.689 (-5.554)	-2.239 (-2.197)	3.450 (3.357)	3.1228 (3.5947)	-4.990	-2.944	2.046	606	0.725 (0.638)	0.681	-0.953 (1.210)
(*Z,Z*)-**7**	-5.294 (-5.319)	-2.428 (-2.461)	2.866 (2.858)	1.4131 (1.7609)	-4.950	-3.113	1.837	670	0.690 (0.446)	0.568	-4.013 (16.620)
(*E,Z*)-**7**	-5.356 (-5.367)	-2.426 (-2.467)	2.930 (2.900)	2.4746 (2.9771)	-4.960	-3.088	1.872	662.5	0.735 (0.558)	0.646	-2.203 (3.956)
(*E,E*)-**7**	-5.417 (-5.413)	-2.423 (-2.465)	2.994 (2.948)	2.4799 (3.0118)	-5.050	-3.171	1.879	660	0.789 (0.574)	0.681	-2.455 (3.019)

[a] Calculated from DFT calculations using B3LYP/6-31G(d) in gas phase (The values in parenthesis are DFT calculated values in DCM phase); [b] Calculated as E_{HOMO} = $-e[E_{ox}^{onset} + 4.4]$ and $E_{LUMO} = E_g^{opt} + E_{HOMO}$ (E_{ox}^{onset} was determined from CV in DCM at 1 x 10^{-4} M in the presence of n-Bu_4NPF_6 (0.025 M) at 100 mVs^{-1}) versus ferrocenium/ferrocene redox couple; [c] calculated from the absorption edge $E_g^{opt} = 1240/\lambda_{edge}$; [d] recorded in DCM (1 x 10^{-5} M); [e] E_{pc} values in parenthesis (E_{pa} Fc = 0.572 V and E_{pc} Fc =0.472 V); [f] Half-wave potential, $E_{1/2}= (E_{pc} + E_{pa})/2$, where E_{pc} and E_{pa} correspond to the cathodic and anodic peak potentials, respectively; ΔE_p = 80–120 mV; and a scan rate of 100 mV s^{-1} ($E_{1/2}$ Fc = 0.522 V). [g] Amplitudes of the anodic and cathodic (in parenthesis) peaks (i_{pa} Fc = -2.116 A and i_{pc} Fc = 2.180 A).

View Article Online
DOI: 10.1039/C6TC03876J

(*E*)-**6** (46 x 10^{-30} esu) (Table 2), which is in good agreement with the calculated dipole moments in gas as well as DCM phases, and the optical band gap (Table 1). This decrease, albeit small, is attributed to the comparatively weaker charge transfer owing to stabilization of the HOMOs (Table 1) in the latter. Further, assuming that these chromophores can be described as one-dimensional dipolar chromophores with a single dominating dipolar β_{ZZZ} tensor component,[51] this tensor component along the molecular z-axis is relevant for these two isomers and has been calculated corresponding to the β_{HRS} from the relation $\beta_{ZZZ} = \beta_{HRS}\ (35/6)^{1/2}$ as 126 x 10^{-30} esu and 111 x 10^{-30} esu (Table 2), respectively for (*Z*)- and (*E*)-**6** isomers. Similarly, in the disubstituted D-A-D chromophore **7**, the observed trend in the β_{HRS} values of its isomers: (*Z,Z*: 132 x 10^{-30} esu) > (*E,Z*: 125 x 10^{-30} esu) > (*E,E*: 96 x 10^{-30} esu) (Table 2), is essentially the same as the wavelength of their maximum absorption as well as increasing band gap (Table 1) in that order. However, unlike isomers of **6**, these are not characterised by a single major charge-transfer axis and thus cannot be classified as one-dimensional chromophores. Therefore β_{ZZZ} hyperpolarizability tensor component could not be calculated. Compared to **6**, the observed increase in the first hyperpolarizability values in the isomers of disubstituted analogues of **7** is attributed to the addition of a second dipolar charge-transfer moiety. But a simplified model could be constructed, if it is assumed that the two dipolar β_{ZZZ} tensor elements add up vectorially in the **7** triads.[52-54] From the crystal structure, at least for (*E,E*)-**7**, vector model could be constructed that allowed calculation of the vector sum of two β_{ZZZ} components in (*E,E*)-**7** from the given expressions,

$$\beta_{ZZZ,0(avg.7)} = 2\ (\cos \theta/2)^3\ \beta_{ZZZ,0\ (avg.6)} \text{ ....(1)}$$

$$\beta_{ZZZ,0(avg.)} = \beta_{HRS,0(avg.)}\ (35/6)^{1/2} \text{ ....(2)}$$

This yielded opening angle (Fig. 5) between the two Fc-A arms in (*E,E*)-**7** to be approx. 44°. Thus, the non-zero value for the opening angle for a D-A-D triad clearly shows that the molecular structure is non-centrosymmetric, which is further corroborated by the crystal structure (Fig. 2d).

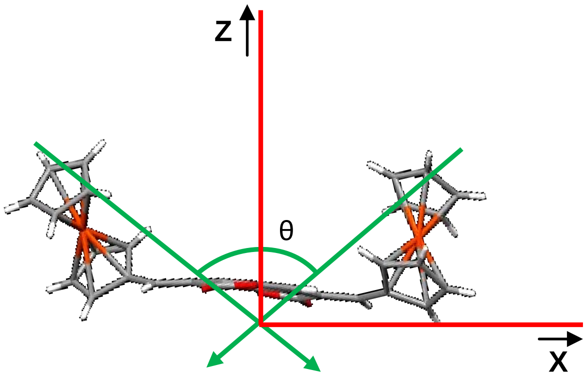

Fig. 5 Representation of opening angle (θ) for (*E,E*)-**7**. Green lines refer to βzzz(mono).

Table 2. Quadratic nonlinear optical parameters for isomers of **6** and **7**.

Comp.	λ_{max}	$\beta_{HRS,1300}$[a] (10^{-30}esu)	β_{ZZZ}[b] (10^{-30} esu)	$\beta_{HRS,0}$[c] (10^{-30}esu)
(*Z*)-**6**	546	52	126	12.6
(*E*)-**6**	526	46	111	13.3
(*Z,Z*)-**7**	582	132	-----	21
(*E,Z*)-**7**	574	125	-----	22
(*E,E*)-**7**	564	96	-----	19

[a] Second-order nonlinear polarizability, β_{HRS} recorded at 1300 nm (10^{-30} esu) in $CHCl_3$. [b] Second-order nonlinear polarizability recorded along molecular z-axis, β_{ZZZ}. [c] Second-order nonlinear polarizability corrected for resonance enhancement, $\beta_{HRS,0}$.

Interesting results are obtained on relating the dynamic $\beta_{HRS,1300}$ to the resonance-corrected $\beta_{HRS,0}$ (Table 2), assuming that the LE (MLCT) band is the single NLO determining band. The close proximity of the MLCT transitions (λ_{LE} = 550 nm approx.) and the second harmonic wavelength (650 nm) resulted in resonantly enhanced values of β.[55,56] To correct the β values for this resonance enhancement, $\beta_{HRS,0}$ was calculated (Table 2) using the simple two-level model by the expression

$$\beta\ (\omega)\ /\ \beta\ (0) = [(\omega_o)^4/(\omega_o^2 - \omega^2)(\omega_o^2 - 4\omega^2)] \text{ ....(3)}$$

where, ω_o is the single photon absorption maximum of the molecule in wave numbers, and ω is the laser fundamental frequency. Comparing the average of the intrinsic β values ($\beta_{HRS,0}$, without resonance enhancement) of the isomers of the dyad **6** with the averaged values of the three isomers of the triad, it could be seen that $\beta_{HRS,0}$ values of the latter are roughly doubled (Table 2).

Charge transport behaviour

The intramolecular charge transfer in the donor-acceptor (D-A) dyads of the types **6** and **7** bearing redox active organometallic species such as Fc as donor linked to appropriate acceptor have been also used as promising semiconducting materials. Although large number of D-A systems have been used in thin film[57-60] as well as single crystal organic field effect transistors (OFETs) devices,[61-70] however, in no instance has a Fc based semiconducting materials used in OFETs. Incorporation of Fc in such chromophores can provide attractive features such as flexibility in molecular design, light weight, low cost, thermal stability apart from redox behaviour, which can induce switching of a function. In the latter context, using spectroelectrochemistry, we previously reported[27,29,30] switching of second-order NLO polarizability of Fc based chromophores as well as demonstrated switching of their NLO response. To test the above hypothesis, and in continuation of our interest,[71-74] we fabricated thin film OFET devices of selected (*E*)-**6** and (*Z,Z*)-**7**. Interestingly, the latter behaves as a stable charge transport material with dominating n-type charge transport. It is worth mentioning that although a number of small molecules based p-channel semiconductor materials have been reported[75-79] with attractive charge carrier

View Article Online
DOI: 10.1039/C6TC03876J

mobility, only a few n-channel[80-83] and even less number of ambipolar materials based on small molecules have been reported.[84-87]

The stronger oxidation peak of (*Z,Z*)-**7** compared to (*E*)-**6** indicated greater p-doping process of the former compared to (*E*)-**6**. Comparison of the calculated energy levels of HOMOs and LUMOs revealed (Table 1) that compared to LUMO (-2.197) in (*E*)-**6**, attachment of second Fc led to lowering of LUMO (-2.461 eV) in (*Z,Z*)-**7**. However, attachment of the second Fc further raised the energy of the HOMO (-5.319 eV), compared to (*E*)-**6** (-5.554 eV) and also led to decrease in the HOMO-LUMO gap (2.858 eV) in (*Z,Z*)-**7**. These results suggested (*Z,Z*)-**7** to be a narrow band gap dyad, compared to (*E*)-**6** (E_g^{calcd} 3.357 eV) as also revealed from the optical band gap (ΔE_g^{opt} 0.209 eV) (Table 1). A similar lowering of the HOMO-LUMO gap of (*E*)-**6** and (*Z,Z*)-**7** (Table 1) compared to that of Fc was also noted.

Further, the experimental HOMO-LUMO energies showed good correlation with the theoretically calculated values (Table 1). For most n-type organic semiconductors, the LUMO levels are in the range -3.5 to -4.0 eV.[88,89] In the present case, while (*E*)-**6** has LUMOs at -2.944 eV, (*Z,Z*)-**7** has lower (-3.113 eV) LUMO levels, which are however optimal for n-type charge transport. Compared to (*E*)-**6**, the lower band gap in (*Z,Z*)-**7** suggests operation of a strong intramolecular charge transfer, which could be attributed to the enhanced π-conjugation owing to the additional Fc donor. Further, since the LUMOs in (*Z,Z*)-**7** are more stabilized compared to (*E*)-**6**, a facile electron injection by the Au electrodes of the OFET device is expected.

FET devices of (*Z,Z*)-**7** obtained from 10 set of measurements clearly showed both n-type and p-type transport characteristics in the $I_d(V_g)$ response with μ_e^{FET} of 3 x 10^{-3} $cm^2V^{-1}s^{-1}$ and μ_h^{FET} of 7 x 10^{-5} $cm^2V^{-1}s^{-1}$ and with *on/off* ratio, $I_{on/off}$ ≈10^3 (Fig. 6a and 6b). However, the field-effect mobility due to holes and electrons is unbalanced and inclined in favour of n-type charge transport. In case of (*E*)-**6**, FET characteristics were not observed, primarily due to the absence of smooth film formation (Fig. 6c), unlike the optical quality films of (*Z,Z*)-**7** (Fig. 6d). The film formation features could possibly be attributed to the molecular packing tendency of these hybrids**.** The X-ray powder diffraction pattern of thin films of (*E*)-**6** and (*Z,Z*)-**7** deposited on silica substrates is shown in (Fig. S37, see †ESI). A slightly broad peak was observed at a d-spacing of 3.84 Å and 3.71 Å for (*E*)-**6** and (*Z,Z*)-**7**, respectively. The AFM height image of (*E*)-**6** showed amorphous network while a slight crystalline network is shown for (*Z,Z*)-**7** with a root mean-square (RMS) deviation of 70.95 nm and 2.42 nm, respectively as shown in (Fig. 6c and 6d). Thus, low mobility values were observed for (*Z,Z)*-**7** while (*E*)-**6** showed no mobility in accordance with the high roughness obtained.[90] Based on the low mobility values of (*Z,Z*)-**7**, we believe that although Fc acts as a good donor, the non-planarity[91] and steric restrictions caused by it in the present systems, might be one of the possible reasons for the lower field-effect mobility.

CONCLUSIONS

We have described intrinsic second-order nonlinear polarizability (quadratic/first hyperpolarizability, *β*) of dyads having Fc donor linked to benzo[1,2-b:4,5-b']difuran-2,6-(3*H*,7*H*)-dione acceptor (D-A type) and the acceptor flanked by two Fc units (D-A-D type).

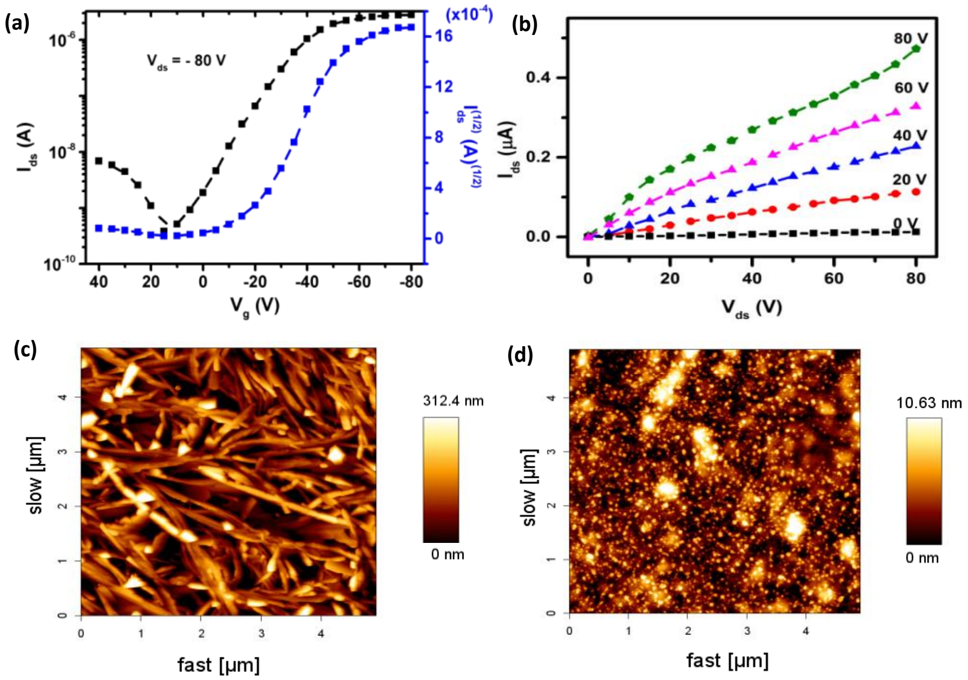

Fig. 6 (a) Representative transfer and (b) output characteristics of (*Z,Z*)-**7** on HDMS passivated BCB dielectric. AFM height images of thin films of (c) (*E*)-**6** and (d) (*Z,Z*)-**7** coated on BCB.

View Article Online
DOI: 10.1039/C6TC03876J

Interestingly, different geometrical isomers of these D-A constructs were isolated, which allowed us to deduce interesting comparisons on the NLO behaviour of these isomeric compounds. Femtosecond HRS measurements were performed at 1300 nm using a commercial Ti:sapphire laser at ambient temperature and revealed structure dependent quadratic hyperpolarizabilities. In UV-visible absorption spectrum, positions of the bands get blue shifted in (*E*)-**6** as compared to its *cis*- counterpart, which has been attributed to the influence of the *trans*- geometry weakening the charge-transfer in (*E*)-**6**, that was in good agreement with the theoretical data. Similar trends were observed in the isomers of **7**. Electrochemical data revealed that (*E*)-**6** isomer shows greater anodic shift than (*Z*)-**6** due to stabilization of the HOMOs of (*E*)-**6** compared to (*Z*)-**6**. Among the isomers of chromophore **7**, the oxidation potential as well as half-wave of the three isomers followed the order: (*Z,Z*) < (*E,Z*) < (*E,E*). Chromophore (*Z*)-**6** recorded higher β_{HRS} than (*E*)-**6**, which is attributed to weaker charge transfer. Similarly, in D-A-D chromophore **7**, β_{HRS} values of isomers follow the order (*Z,Z*) > (*E,Z*) > (*E,E*), which matches with trend noted in the wavelength of their maximum absorption as well as increasing band gap in that order. Thus, a good correlation of the structural changes of these isomers as well with the experimental β-values was established. Further, the triad (*Z,Z*)-**7** exhibited moderate electron as well as hole mobility. Further, structural modifications could possibly improve the semiconducting characteristics of such multifunctional systems.

Acknowledgements

This work was supported by SERB-DST, New Delhi for financial assistance (project SB/S1/OC-45/2013) to KS. Authors also thank Guru Nanak Dev University, Amritsar (UPE Programme) for facilities. We also thank single crystal X-ray diffraction facility at IIT Indore for determining the single crystal X-ray structures.

Notes and References

1 X. Zhang, Z. Chi, B. Xu, L. Jiang, X. Zhou, S. Liu and J. Xu, *Chem. Commun.* 2012, **48**, 10895-10897.
2 Y. Lei, P. Deng, J. Li, M. Lin, F. Zhu, T.-W. Ng, C.-S. Lee and B. S. Ong, *Sci. Rep.* 2016, **6**, 24476; doi: 10.1038/srep24476.
3 A.-J. Payne, A. D. Hendsbee, S. M. McAfee, D. K. Paul, K. Karan and G. C. Welch, *Phys. Chem. Chem. Phys.*, 2016, **18**, 14709-14719.
4 D. R. Kanis, M. A. Ratner and T. J. Marks, *Chem. Rev.*, 1994, **94**, 195–242.
5 S. R. Marder, B. Kippelen, A. K.-Y. Jen and N. Peyghambarian, *Nature*, 1997, **388**, 845–851.
6 I. R. Whittall, A. M. McDonagh, M. G. Humphrey and M. Samoc, *Adv. Organomet. Chem.*, 1998, **42**, 291–362.
7 K. A. Green, M. P. Cifuentes, M. Samoc and M. G. Humphrey, *Coord. Chem. Rev.*, 2011, **255**, 2025–2038.
8 P. N. Prasad and D. J. Williams, *Nonlinear Optical Effects in Molecules and Polymers*, Wiley, New York, 1991.
9 P. N. Prasad, *Nonlinear Optical Properties of Organic Materials*, Plenum, New York, 1991.
10 P. N. Prasad, *Nanophotonics*, Wiley, New York, 2004.
11 R. W. Boyd, *Nonlinear Optics*, Academic Press, New York, 1992.
12 Y. Shirota, *J. Mater. Chem.*, 2000, **10**, 1–25.
13 K. Clays, *Chem. Mater.*, 2003, **15**, 642–648.
14 M. G. Kuzyk, *J. Mater. Chem.*, 2009, **19**, 7444–7465.
15 S. Barlow and S. R. Marder, *Chem. Commun.*, 2001, 1555–1562.
16 P. Debroy and S. Roy, *Coord. Chem. Rev.*, 2007, **251**, 203–221.
17 R. Horikoshi and T. Mochida, *Eur. J. Inorg. Chem.*, 2010, 5355–5371.
18 F. Paul, K. Costuas, I. Ledoux, S. Deveau, J. Zyss, J.- F. Halet and C. Lapinte, *Organometallics*, 2002, **21**, 5229-5235.
19 T. Weyland, I. Ledoux, S. Brasselet, J. Zyss, and C. Lapinte, *Organometallics*, 2000, **19**, 5235-5237.
20 M. Samoc, N. Gauthier, M. P. Cifuentes, F. Paul, C. Lapinte and M. G. Humphrey, *Angew. Chem. Int. Ed.*, 2006, **45,** 7376-7379.
21 M. L. H. Green, S. R. Marder, M. E. Thompson, J. A. Bandy, D. Bloor, P. V. Kolinsky and R. J. Jones, *Nature*, 1987, **330**, 360-362.
22 B. J. Coe, R. J. Docherty, S. P. Foxon, E. C. Harper, M. Helliwell, J. Raftery, K. Clays, E. Franz and B. S. Brunschwig, *Organometallics*, 2009, **28**, 6880-6892.
23 C. Sporer, I. Ratera, D. Ruiz-Molina, Y. Zhao, J. Vidal-Gancedo, K. Wurst, P. Jaitner, K. Clays, A. Persoons, C. Rovira and J. Veciana, *Angew. Chem.*, *Int. Ed.*, 2004, **43**, 5266–5268.
24 B. J. Coe, *Acc. Chem. Res.*, 2006, **39**, 383–393.
25 P. Kaur, M. Kaur, G. Depotter, S. van Cleuvenbergen, I. Asselberghs, K. Clays and K. Singh, *J. Mater. Chem.*, 2012, **22**, 10597–10608.
26 W.-Y. Wang, N.-N. Ma, S.-L. Sun and Y.-Q. Qiu, *Phys. Chem. Chem. Phys.*, 2014, **16**, 4900–4910.
27 S. Kaur, S. Dhoun, G. Depotter, P. Kaur, K. Clays and K. Singh, *RSC Adv.*, 2015, **5**, 84643–84656.
28 S. Dhoun, G. Depotter, S. Kaur, P. Kaur, K. Clays and K. Singh, *RSC Adv.*, 2015, **6**, 50688–50696.
29 J. Chiffre, F. Averseng, G. G. A. Balavoine, J.- C. Daran, G. Iftime, P. G. Lacroix, E. Manoury and K. Nakatani*, Eur. J. Inorg. Chem.,* 2001, **9**, 2221-2226.
30 J. A. Mata, E. Peris, R. Llusar, S. Uriel, M. P. Cifuentes, M. G. Humphrey, M. Samoc and B. L. Davies, *Eur. J. Inorg. Chem.,* 2001, **8**, 2113-2122.
31 J. A. Mata, E. Peris, R. Llusar and E. Peris, *Organometallics,* 2000, **19***,* 3797-3802.
32 H. K. Sharma, K. H. Pannell, I. Ledoux, J. Zyss, A. Ceccanti and P. Zanello, *Organometallics,* 2000, **19***,* 770-774.
33 J. A. Mata, E. Peris, I. Asselberghs, R. Van Boxel and A. Persoons, *New J. Chem.*, 2001, **25**, 1043-1046.
34 J. A. Mata, E. Peris, I. Asselberghs, R. Van Boxel *and* A. Persoons, *New J. Chem.*, 2001, **25**, 299-304.
35 K. Clays and A. Persoons, *Phys. Rev. Lett.*, 1991, **66**, 2980–2983.
36 K. Clays and A. Persoons, *Rev. Sci. Instrum.*, 1992, **63**, 3285–3289.
37 K. Clays, A. Persoons and L. De Maeyer, *Adv. Chem. Phys.*,1994, **85**, 455–498.
38 K. Clays and A. Persoons, *Rev. Sci. Instrum.*, 1994, **65**, 2190–2194.
39 G. Olbrechts, R. Strobbe, K. Clays and A. Persoons, *Rev. Sci. Instrum.*, 1998, **69**, 2233–2241.
40 G. Olbrechts, K. Wostyn, K. Clays and A. Persoons, *Opt. Lett.*, 1999, **24**, 403–405.
41 T. Verbiest, S. Houbrechts, M. Kauranen, K. Clays and A. Persoons, *J. Mater. Chem.*, 1997, **7**, 2175–2189.

42 S. D. Bella, *Chem. Soc. Rev.*, 2001, **30**, 355–366.

43 H. M. Kim and B. R. Cho, *J. Mater. Chem.*, 2009, **19**, 7402–7409.

44 M. J. Frisch, et al., Gaussian 09, Revision B.01, Gaussian, Inc., Wallingford, CT, 2010 (for complete reference see ESI†).

45 C. Adamo and D. Jacquemin, *Chem. Soc. Rev.* 2013, **42**, 845-856.

46 S. M. Islam, S. D. Huelin, M. Dawe and R. A. Poirier, *J. Chem. Theory Comput.* 2008, **4**, 86-100.

47 T. Lei, J. H. Dou, X. Y. Cao, J. Y. Wang and J. Pei, *J. Am. Chem. Soc.*, 2013, **135**, 12168-12171.

48 Z. Yan, B. Sun and Y. Li, *Chem. Commun.* 2013, **49**, 3790-3792.

49 B. Sun, W. Hong, E. Thibau, H. Aziz, Z. H. Lu and Y. Li, *Org. Electron.*, 2014, **15**, 3787-3794.

50 J. H. Wood and L. Cox. *Organic Syntheses. Coll.*, 1955, **3**, 286 ; 1946, **26**, 24.

51 C. H. Wang, Y. C. Lin, O. Y. Tai, and A. K.-Y. Jen, *J. Chem. Phys.*, 2003, **119**, 6237-6244.

52 G. Hennrich, M. T. Murillo, P. Prados, K. Song, I. Asselberghs, K. Clays, A. Persoons, J. B. Buchholz and J. De Mendoza, *Chem. Commun.*, 2005, 2747–2749.

53 G. Hennrich, M. T. Murillo, P. Prados, H. Al-Saraierh, A. El-Dali, D. W. Thompson, J. Collins, P. E. Georghiou, A. Teshome, I. Asselberghs and K. Clays, *Chem. Eur. J.*, 2007, 13, 7753– 7761.

54 E. Hendrickx, C. Boutton, K. Clays, A. Persoons, S. Van Es, T. Biemans, B. Meijer, *Chem. Phys. Lett.*, 1997, **270**, 241-244.

55 C. A. Van Walree, O. Franssen, A. W. Marsman, M. C. Flipse and L. W. Jenneskens, *J. Chem. Soc., Perkin Trans.*, 1997, **2**, 799-807.

56 S. H. Mashraqui, R. S. Kenny, S. G. Ghadigaonkar, A. Krishnan, M. Bhattacharya, P. K. Das, *Opt. Mater.*, 2004, **27**, 257–260.

57 F. Fungo, L. Otero, C. D. Borsarelli, E. N. Durantini, J. J. Silber and L. Sereno, *J. Phys. Chem. B.*, 2002, **106**, 4070-4078.

58 D. M. Guldi, C. Luo, D. Koktysh, N. A. Kotov, T. D. Ros, S.Bosi and M. Prato, *Nano Lett.*, 2002, **2**, 775-780.

59 C. E. Mauldin, C. Piliego, D. Poulsen, D. A. Unruh, C. Woo, B. Ma, J. L. Mynar and J. M. J. Frechet, *Applied Materials and interfaces*, 2010, **2**, 2833-2838.

60 A. W. Hains, Z. Liang, M. A. Woodhouse and B. A. Gregg, *Chem. Rev.*, 2010, **110**, 6689-6735.

61 C. D. Dimitrakopoulos and P. R. L. Malenfant, *Adv. Mater.*, 2002, **14**, 99-117.

62 H. Meng, F. Sun, M. B. Goldfinger, F. Gao, D. J. Londono, W. J. Marshal, G. S. Blackman, K. D. Dobbs, E. Dalen and D. E. Keys, *J. Am. Chem. Soc.*, 2006, **128**, 9304-9305.

63 D. Cahen and G. Hodes, *Adv. Mater.*, 2002, **14**, 789-798.

64 K. Singh, A. Sharma, J. Zhang, W. Xu and D. Zhu, *Chem. Commun.*, 2011, **47**, 905-907.

65 T. Zhao, Z. Wei, Y. Song, W. Xu, W. Hu and D. Zhu, *J. Mater. Chem.*, 2007, **17**, 4377-4381.

66 J. M. Mativetsky, M. Kastler, R. C. Savage, D. Gentilini, M. Palma, W. Pisula, K. Mullen and P. Samorı, *Adv. Funct. Mater.*, 2009, **19**, 2486-2494.

67 A. Mishra, C. Q. Ma and P. Bauerle, *Chem. Rev.*, 2009, **109**, 1141-1276.

68 L. E. Polander, S. P. Tiwari, L. Pandey, B. M. Seifried, Q. Zhang, S. Barlow, C. Risko, J. L. Bredas, B. Kippelen and S. R. Marder, *Chem. Mater.*, 2011, **23**, 3408-3410.

69 S. Wang, A. Kiersnowski, W. Pisula and K. Mullen, *J. Am. Chem. Soc.*, 2012, **134**, 4015-4018.

70 M. S. Chen, J. R. Niskala, D. A. Unruh, C. K. Chu, O. P. Lee and J. M. J. Freechet, *Chem. Mater.*, 2013, **25**, 4088-4096.

71 K. Singh, T. S. Virk, J. Zhang, W. Xu and D. Zhu, *Chem. Commun.*, 2012, **48**, 12174-12176.

72 K. Singh, T. S. Virk, J. Zhang, W. Xu and D. Zhu, *Chem. Commun.*, 2012, **48**, 121-123.

73 J. Zhang, J. Tan, Z. Ma, W. Xu, G. Zhao, H. Geng, C. Di, W. Hu, Z. Shuai, K. Singh and D. Zhu, *J. Am. Chem. Soc.*, 2013, **135**, 558-561.

74 J. Zhang, H. Geng, T. S. Virk, Y. Zhao, J. Tan, C. A. Di, W. Xu, K. Singh, W. Hu, Z. Shuai, Y. Liu and D. Zhu, *Adv. Mater.*, 2012, **24**, 2603-2607

75 M. M. Payne, S. R. Parkin, J. E. Anthony, C. C. Kuo and T. N. Jackson, *J. Am. Chem. Soc.*, 2005, **127**, 4986-4987.

76 Y. Zhu, R. D. Champion and S. A. Jenekhe, *Macromolecules*, 2006, **39**, 8712-8719.

77 P. Qin, H. Zhu, T. Edvinsson, G. Boschloo, A. Hagfeldt and L. Sun, *J. Am. Chem. Soc.*, 2008, **130**, 8570-8571.

78 Y. Li, S. P. Singh and P. A. Sonar, *Adv. Mater.*, 2010, **22**, 4862-4866.

79 J. S. Ha, K. H. Kim and D. H. Choi, *J. Am. Chem. Soc.*, 2011, **133**, 10364-10367.

80 A. Facchetti, J. Letizia, M. H. Yoon, M. Mushrush, H. E. Katz and T. J. Marks, *Chem. Mater.*, 2004, **16**, 4715-4727.

81 T. Kono, D. Kumaki, J. I. Nishida, T. Sakanoue, M. Kakita, H. Tada, S. Tokito and Y. Yamashita, *Chem. Mater.*, 2007, **19**, 1218-1220.

82 R. Schmidt, J. H. Oh, Y. S. Sun, M. Deppisch, A. M. Krause, K. Radacki, H. Braunschweig, M. Konemann, P. Erk, Z. Bao and F. Wurthner, *J. Am. Chem. Soc.*, 2009, **131**, 6215-6228.

83 X. Gao, C. A. Di, Y. Hu, X. Yang, H. Fan, F. Zhang, Y. Liu, H. Li and D. Zhu, *J. Am. Chem. Soc.*, 2010, **132**, 3697-3699.

84 A. P. Kulkarni, Y. Zhu, A. Babel, P. T. Wu and S. A. Jenekhe, *Chem. Mater.*, 2008, **20**, 4212-4223.

85 J. C. Bijleveld, A. P. Zoombelt, S. G. J. Mathijssen, M. M. Wienk, M. Turbiez, D. M. D. Leeuw and R. A. J. Janssen, *J. Am. Chem. Soc.*, 2009, **131**, 16616-16617.

86 F. S. Kim, X. Guo, M. D. Watson and S. A. Jenekhe, *Adv. Mater.*, 2010, **22**, 478-482.

87 S. Cho, J. Lee, M. Tong, J. H. Seo and C. Yang, *Adv. Funct. Mater.*, 2011, **21**, 1910-1916.

88 A. Wan, J. Hwang, F. Amy and A. Kahn, *Org. Electron.*, 2005, **6**, 47-54.

89 S. Braun, W. R. Salaneck and M. Fahlman, *Adv. Mater.*, 2009, **21**, 1450-1472.

90 S. Steudel, S. D. Vusser, S. D. Jonge, D. Janssen, S. Verlaak, J. Genoe and P. Heremans, *Appl. Phys. Lett.*, 2004, **85**, 4400-4402.

91 T. Hasegawa, M. Ashizawa and H. Matsumoto, *RSC Adv.*, 2015, **5**, 61035-61043.

View Article Online
DOI: 10.1039/C6TC03876J

Multifunctional geometrical isomers of ferrocene-benzo[1,2-*b*:4,5-*b′*]difuran-2,6-(3*H*,7*H*)-dione adducts: Second-order nonlinear optical behaviour and charge transport in thin film OFET devices

Priya Singla,[a] Nick Van Steerteghem,[b] Navdeep Kaur,[a] A. Z. Ashar,[c] Paramjit Kaur,*,[a] Koen Clays,[b] K. S. Narayan[c] and Kamaljit Singh*,[a]

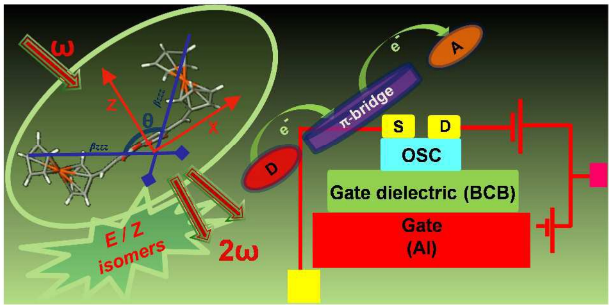

New ferrocene based donor-acceptor chromophores depict structure dependent second-order nonlinear polarizability and charge transport in thin film OFET devices.